Optical Engineering

OpticalEngineering.SPIEDigitalLibrary.org

Self-calibration method based on navigation in high-precision inertial navigation system with fiber optic gyro

Lei Wang
Wei Wang
Qian Zhang
Pengyu Gao

SPIE.

Self-calibration method based on navigation in high-precision inertial navigation system with fiber optic gyro

Lei Wang,* Wei Wang, Qian Zhang, and Pengyu Gao
Beihang University, School of Instrumentation Science and Opto-electronics Engineering, #37 Xueyuan Road, Haidian District, Beijing, 100191 China

Abstract. A rotary inertial navigation system requires higher calibration accuracy of some error parameters owing to rotation. Conventional multiposition and rotation calibration methods are limited, for they do not consider sensors' actual operating condition. In order to achieve these parameters' values as closely as possible to their true values in application, their influence on navigation is analyzed, and a relevant new calibration method based on a system's velocity output during navigation is designed for the vital error parameters, including inertial sensors' installation errors and the scale factor error of fiber optic gyro. Most importantly, this approach requires no additional devices compared to the conventional method and costs merely several minutes. Experimental results from a real dual-axis rotary fiber optic gyro inertial navigation system demonstrate the practicability and higher precision of the suggested approach. [DOI: 10.1117/1.OE.53.6.064103]

Keywords: self-calibration method; fiber optic gyro; rotary inertial navigation system.

Paper 140545 received Apr. 1, 2014; revised manuscript received May 20, 2014; accepted for publication May 30, 2014; published online Jun. 25, 2014.

1 Introduction

It has becomes a trend that fiber optic gyro (FOG) is employed in inertial navigation systems (INS) due to its low cost, small size, low power consumption, and high reliability.[1,2] Rotating inertial measurement units (IMU) periodically can bound the free propagation of the INS error introduced by gyro drift.[3,4] Thus, this method is applied to improve the precision of FOG INS. As a single-axis rotary INS has an effect on only two gyros,[5,6] one more rotation axis should be added at least to reduce the impact of all three gyros and achieve higher precision of navigation results.[7,8] A typical rotation strategy of dual-axis rotary INS is presented in Ref. 9. But this strategy plays an equal role in the three gyros named x, y, and z. Compared to gyro z, the drifts of gyros x and y contribute more to the system's inaccuracy during navigation. This paper examines a dual-axis rotary FOG INS with a new rotation strategy that rotates several circles along with the z axis to bound the drifts of gyros x and y and then quickly rotates 180 deg along the x axis to reduce the impact of gyro z's drift, by which the drifts of gyros x and y can be mitigated more efficiently. For the change of rotation strategy, the influence of error parameters on navigation is diverse and the calibration associated with this should be redesigned.

Calibration is required by any type of INS.[10] For the novel system proposed in this paper, because of its particular rotation, a more precise calibration is demanded for the gyro's scale factor and some special installation error parameters. Conventional calibration, named multiposition and rotation method, generally, is carried out with the support of external turn tables.[11,12] However, many error parameters are related to environmental conditions. The positions and rotational movements that the turn table affords differ from the actual operating condition of INS; hence, the values of error parameters calibrated by the method above are not accurate enough for system requiremenst. Especially for FOG INS, a gyro's performance is more susceptible to environmental conditions, such as temperature,[13,14] magnetic field,[15] and vibration.[16] Therefore, for the sake of high-precision, conventional multiposition and rotation method is treated as a basic calibration in the proposed INS, and a precise calibration considering the sensors' actual operating condition is required.

Thus, a calibration based on the velocity error of navigation in a stationary base is designed to decrease the impact due to environmental conditions. What is more, this calibration method does not need the utilization of external high-accuracy turn tables. All in all, compared with a conventional multiposition and rotation method, this calibration meets system requirements of better accuracy in performance and brings a sharp decrease in cost.

The rest of the paper is organized as follows. Section 2 examines the error parameters in this system. The mathematical models between error parameters and velocity errors are established for the calibration in Sec. 3. Section 4 presents and discusses the experimental calibration results, followed by conclusions in Sec. 5.

2 Analysis of Error Parameters

There is no doubt that sensor error exists in inertial systems. In this paper, gyro and accelerometer's scale factor errors are symbolized as ΔK_{gx}, ΔK_{gy}, ΔK_{gz}, ΔK_{ax}, ΔK_{ay}, and ΔK_{az}. Gyro drifts are symbolized as ε_x, ε_y, and ε_z. Accelerometer biases are symbolized as ∇_x, ∇_y, and ∇_z.

*Address all correspondence to: Lei Wang, E-mail: 351722wang@163.com

Misalignment angles due to installation account for the system's navigation inaccuracy as well. Especially for rotary INS, they are different from those in common INS. To define these installation errors, except for two common coordinate frames called a body frame (denoted as b) and a navigation frame (denoted as n), another two essential coordinate frames and their relationship must also be illustrated. One is the inertial sensor axes frame (denoted as a) that is defined by the sensors' input axes. Because it is unrealistic that gyros and accelerometers of the IMU are mounted orthogonally without any error, a-frame is a nonorthogonal coordinate frame. In contrast, the other one, called the IMU frame (denoted as s), is an orthogonal coordinate frame. First of all, sensors' output should be transformed from a-frame to s-frame. As an s-frame varies with the real-time attitudes of IMU in rotary INS, data should be transformed to n-frame, which is a local-level frame with orientation east-north-up in this paper, for navigation calculation subsequently, and b-frame is used for attitude calculation.

The Z_s axis of the s-frame is defined to coincide with the inner rotation axis of this dual-axis rotary INS. Then, the X_s axis is defined by the projection of X_a in the normal plane of Z_s, and the Y_s axis is defined according to the right-hand rule. Therefore, the misalignment of gyros can be presented by five small angles β_{gx}, β_{gy}, α_{gy}, δ_{gzX}, and δ_{gzY}, as shown in Fig. 1. Then the direction cosine matrix required to transform the gyro data from a-frame to s-frame can be simplified as

$$C_{ag}^{s} = \begin{bmatrix} 1 & 0 & \beta_{gx} \\ \alpha_{gy} & 1 & -\beta_{gy} \\ -\delta_{gzY} & \delta_{gzX} & 1 \end{bmatrix}. \tag{1}$$

Similarly, the direction cosine matrix required to transform the accelerometer data from a-frame to s-frame can be simplified as

$$C_{aa}^{s} = \begin{bmatrix} 1 & -\alpha_{ax} & \beta_{ax} \\ \alpha_{ay} & 1 & -\beta_{ay} \\ -\delta_{azY} & \delta_{azX} & 1 \end{bmatrix}, \tag{2}$$

where symbols β_{ax}, β_{ay}, α_{ax}, α_{ay}, δ_{azX}, and δ_{azY} also represent six small angles.

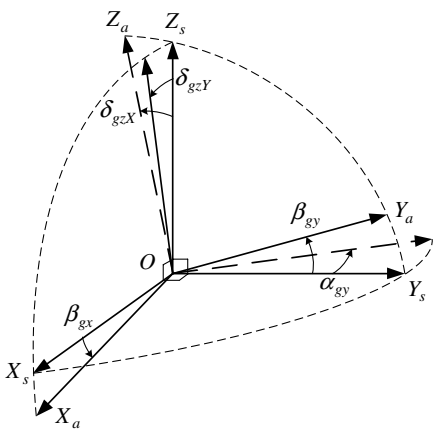

Fig. 1 Installation error of gyros.

3 Principle of the Navigation-Based Self-Calibration Method

3.1 *Models of Navigation Error in Calibration*

For systems studied in this paper, except the misalignment angles α_{ax} and α_{ay}, the rough values of other error parameters mentioned in Sec. 2 can be calibrated and compensated easily by conventional methods before navigation calculations, which makes this calibration based on navigation both necessary and feasible. On one hand, as the spatial relationship between gyros and accelerometers is hard to ascertain without system-level methods, α_{ax} and α_{ay} that are defined by taking x gyro as the reference in this paper, are not calibrated separately in the preceding conventional method. The conventional calibration obtained here is merely the difference of α_{ax} and α_{ay} so that to get their respective value by navigation is obligatory. On the other hand, if there is no conventional calibration and compensation reducing error in parameters' value beforehand, it is difficult to separate them from each other.

Since the status of IMU in alignment is rotating along with the Z_s axis, when IMU taking the same action in navigation, most error parameters are balanced with alignment error and can hardly be calibrated. Additionally, velocity output in stationary base navigation should be zero in theory. Thus, this paper focuses on a system's velocity output when IMU rotates 180 deg along with the X_s axis. As shown in Fig. 2, the direction cosine matrix required to transform inertial sensor data from s-frame to b-frame in this course is

$$C_{s}^{b} = \begin{bmatrix} 1 & 0 & 0 \\ 0 & \cos\omega t & -\sin\omega t \\ 0 & \sin\omega t & \cos\omega t \end{bmatrix}. \tag{3}$$

During the calibration, INS is placed with its b-frame coincident with the n-frame, approximately. So the direction cosine matrix required to transform inertial sensor data from b-frame to n-frame can be written as

$$C_{b}^{n} = I_{3\times3}. \tag{4}$$

When the IMU starts to rotate along with X_s axis, taking no account of any error parameter, the output of inertial sensors can be expressed by Eqs. (5) and (6).

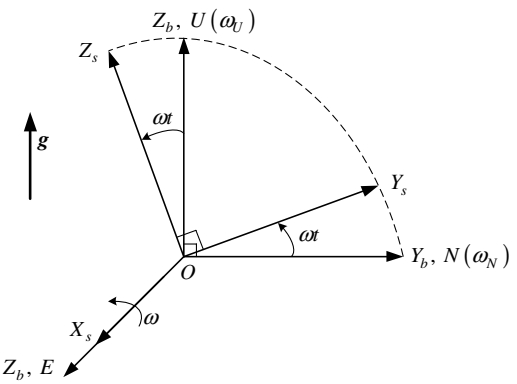

Fig. 2 Relations among coordinate frames.

$$\omega^a = \begin{bmatrix} \omega \\ \omega_N \cos \omega t + \omega_U \sin \omega t \\ \omega_U \cos \omega t - \omega_N \sin \omega t \end{bmatrix}, \tag{5}$$

$$f^a = \begin{bmatrix} 0 \\ g \sin \omega t \\ g \cos \omega t \end{bmatrix}, \tag{6}$$

where ω^a and f^a are the output of gyros and accelerometers, respectively. ω is the angular velocity that IMU rotates along with the X_s axis. ω_N and ω_U denote the north and up components of Earth rotation angular velocity, respectively. g denotes the gravity acceleration.

The calibration takes only a few minutes so that the impact of gyro drift and accelerometer bias on the system's velocity output is a drop in the bucket. Furthermore, there is a continuous large input only for x gyro in this process. So no sensor error other than the scale factor of x gyro can make a difference and be calibrated. Then Eq. (5) is updated as

$$\omega^a = \begin{bmatrix} (1 + \Delta K_{gx})\omega \\ \omega_N \cos \omega t + \omega_U \sin \omega t \\ \omega_U \cos \omega t - \omega_N \sin \omega t \end{bmatrix}. \tag{7}$$

With the analysis above, the measured angular velocity ω^n in n-frame is shown.

$$\begin{aligned} \omega^n &= C_b^n C_s^b C_{ag}^s \omega^a \\ &= \begin{bmatrix} 1 & 0 & 0 \\ 0 & 1 & 0 \\ 0 & 0 & 1 \end{bmatrix} \begin{bmatrix} 1 & 0 & 0 \\ 0 & \cos \omega t & -\sin \omega t \\ 0 & \sin \omega t & \cos \omega t \end{bmatrix} \begin{bmatrix} 1 & 0 & \beta_{gx} \\ \alpha_{gy} & 1 & -\beta_{gy} \\ -\delta_{gzY} & \delta_{gzX} & 1 \end{bmatrix} \begin{bmatrix} (1 + \Delta K_{gx})\omega \\ \omega_N \cos \omega t + \omega_U \sin \omega t \\ \omega_U \cos \omega t - \omega_N \sin \omega t \end{bmatrix} \\ &= \begin{bmatrix} (1 + \Delta K_{gx})\omega + \beta_{gx}(\omega_U \cos \omega t - \omega_N \sin \omega t) \\ \alpha_{gy}(1 + \Delta K_{gx})\omega \cos \omega t + \omega_N - \beta_{gy}(\omega_U \cos^2 \omega t - \omega_N \sin \omega t \cos \omega t) + \delta_{gzY}(1 + \Delta K_{gx})\omega \sin \omega t \\ \quad - \delta_{gzX}(\omega_N \sin \omega t \cos \omega t + \omega_U \sin^2 \omega t) \\ \alpha_{gy}(1 + \Delta K_{gx})\omega \sin \omega t + \omega_U - \beta_{gy}(\omega_U \sin \omega t \cos \omega t - \omega_N \sin^2 \omega t) - \delta_{gzY}(1 + \Delta K_{gx})\omega \cos \omega t \\ \quad + \delta_{gzX}(\omega_N \cos^2 \omega t + \omega_U \sin \omega t \cos \omega t) \end{bmatrix}. \end{aligned} \tag{8}$$

Similarly, the measured acceleration f^n in n-frame is

$$\begin{aligned} f^n &= C_b^n C_s^b C_{aa}^s f^a \\ &= \begin{bmatrix} 1 & 0 & 0 \\ 0 & 1 & 0 \\ 0 & 0 & 1 \end{bmatrix} \begin{bmatrix} 1 & 0 & 0 \\ 0 & \cos \omega t & -\sin \omega t \\ 0 & \sin \omega t & \cos \omega t \end{bmatrix} \begin{bmatrix} 1 & -\alpha_{ax} & \beta_{ax} \\ \alpha_{ay} & 1 & -\beta_{ay} \\ -\delta_{azY} & \delta_{azX} & 1 \end{bmatrix} \begin{bmatrix} 0 \\ g \sin \omega t \\ g \cos \omega t \end{bmatrix} \\ &= \begin{bmatrix} -\alpha_{ax} g \sin \omega t + \beta_{ax} g \cos \omega t \\ -\beta_{ay} g \cos^2 \omega t - \delta_{azX} g \sin^2 \omega t \\ g - \beta_{ay} g \sin \omega t \cos \omega t + \delta_{azX} g \sin \omega t \cos \omega t \end{bmatrix}. \end{aligned} \tag{9}$$

But the true angular velocity ω_0^n and acceleration f_0^n during this time in n-frame are

$$\omega_0^n = \begin{bmatrix} \omega \\ \omega_N \\ \omega_U \end{bmatrix}, \tag{10}$$

$$f_0^n = \begin{bmatrix} 0 \\ 0 \\ g \end{bmatrix}. \tag{11}$$

So, based on Eqs. (8) and (10), the angular velocity measurement error $\Delta\omega^n$ can be described as

$$\Delta\omega^n = \omega^n - \omega_0^n = \begin{bmatrix} \Delta\omega_E \\ \Delta\omega_N \\ \Delta\omega_U \end{bmatrix}, \tag{12}$$

where

$$\begin{cases} \Delta\omega_E = \Delta K_{gx}\omega + \beta_{gx}(\omega_U \cos \omega t - \omega_N \sin \omega t) \\ \Delta\omega_N = \alpha_{gy}(1 + \Delta K_{gx})\omega \cos \omega t \\ \qquad - \beta_{gy}(\omega_U \cos^2 \omega t - \omega_N \sin \omega t \cos \omega t) \\ \qquad + \delta_{gzY}(1 + \Delta K_{gx})\omega \sin \omega t \\ \qquad - \delta_{gzX}(\omega_N \sin \omega t \cos \omega t + \omega_U \sin^2 \omega t) \\ \Delta\omega_U = \alpha_{gy}(1 + \Delta K_{gx})\omega \sin \omega t \\ \qquad - \beta_{gy}(\omega_U \sin \omega t \cos \omega t - \omega_N \sin^2 \omega t) \\ \qquad - \delta_{gzY}(1 + \Delta K_{gx})\omega \cos \omega t \\ \qquad + \delta_{gzX}(\omega_N \cos^2 \omega t + \omega_U \sin \omega t \cos \omega t) \end{cases}. \tag{13}$$

As every error parameter is infinitesimal, the product of them, such as $\alpha_{gy}\Delta K_{gx}$, is a higher-order infinitesimal that can be ignored. Then Eq. (13) is simplified as

$$\begin{cases} \Delta\omega_E = \Delta K_{gx}\omega + \beta_{gx}(\omega_U \cos\omega t - \omega_N \sin\omega t) \\ \Delta\omega_N = \alpha_{gy}\omega \cos\omega t - \beta_{gy}(\omega_U \cos^2\omega t - \omega_N \sin\omega t \cos\omega t) + \delta_{gzY}\omega \sin\omega t - \delta_{gzX}(\omega_N \sin\omega t \cos\omega t + \omega_U \sin^2\omega t) \\ \Delta\omega_U = \alpha_{gy}\omega \sin\omega t - \beta_{gy}(\omega_U \sin\omega t \cos\omega t - \omega_N \sin^2\omega t) - \delta_{gzY}\omega \cos\omega t + \delta_{gzX}(\omega_N \cos^2\omega t + \omega_U \sin\omega t \cos\omega t) \end{cases} . \quad (14)$$

In a similar way, based on Eqs. (9) and (11), the acceleration measurement error Δf^n can be described as

$$\Delta f^n = f^n - f_0^n = \begin{bmatrix} \Delta f_E \\ \Delta f_N \\ \Delta f_U \end{bmatrix}, \quad (15)$$

where

$$\begin{cases} \Delta f_E = -\alpha_{ax} g \sin\omega t + \beta_{ax} g \cos\omega t \\ \Delta f_N = -\beta_{ay} g \cos^2\omega t - \delta_{azX} g \sin^2\omega t \\ \Delta f_U = -\beta_{ay} g \sin\omega t \cos\omega t + \delta_{azX} g \sin\omega t \cos\omega t \end{cases} . \quad (16)$$

The angle errors engendered in this course can be obtained by integrating Eq. (14), as described by Eq. (17). The up component of angle errors is neither listed below nor employed in this calibration, because its impact on velocity cannot come to light in the next short calibration time IMU rotating along with Z_s axis, especially when there is no translocation for the system.

$$\begin{cases} \Delta\phi_E = \int_0^{\pi/\omega} \Delta\omega_E \mathrm{d}t \\ \quad = \Delta K_{gx} \int_0^{\pi/\omega} \omega \mathrm{d}t + \beta_{gx}\omega_U \int_0^{\pi/\omega} \cos\omega t \mathrm{d}t \\ \quad\quad - \beta_{gx}\omega_N \int_0^{\pi/\omega} \sin\omega t \mathrm{d}t \\ \quad = \Delta K_{gx}\pi - \frac{2\beta_{gx}\omega_N}{\omega} \\ \Delta\phi_N = \int_0^{\pi/\omega} \Delta\omega_N \mathrm{d}t \\ \quad = \alpha_{gy}\omega \int_0^{\pi/\omega} \cos\omega t \mathrm{d}t - \frac{\beta_{gy}\omega_U}{2} \int_0^{\pi/\omega} (1+\cos 2\omega t)\mathrm{d}t \\ \quad\quad + \frac{\beta_{gy}\omega_N}{2} \int_0^{\pi/\omega} \sin 2\omega t \mathrm{d}t + \delta_{gzY}\omega \int_0^{\pi/\omega} \sin\omega t \mathrm{d}t \\ \quad\quad - \frac{\delta_{gzX}\omega_N}{2} \int_0^{\pi/\omega} \sin 2\omega t \mathrm{d}t - \frac{\delta_{gzX}\omega_U}{2} \int_0^{\pi/\omega} (1-\cos 2\omega t)\mathrm{d}t \\ \quad = -\frac{\beta_{gy}\omega_U \pi}{2\omega} + 2\delta_{gzY} - \frac{\delta_{gzX}\omega_U \pi}{2\omega} \end{cases} , \quad (17)$$

where $\Delta\phi_E$ and $\Delta\phi_N$ express the east and north components of angle errors.

According to inertial navigation theory, $\Delta\phi_E$ and $\Delta\phi_N$ will cause the increase of horizontal velocity errors directly and observably. As the following period IMU rotating along with the Z_s axis is so short in this paper, the impact caused by $\Delta\phi_E$ and $\Delta\phi_N$ can be described by Eq. (18) for simplicity.

$$\begin{cases} \Delta V_E = -\int_0^t \Delta\phi_N g \mathrm{d}t = -\Delta\phi_N g t \\ \Delta V_N = \int_0^t \Delta\phi_E g \mathrm{d}t = \Delta\phi_E g t \end{cases} , \quad (18)$$

where ΔV_E and ΔV_N express the east and north components of velocity errors.

The velocity errors caused in this course can be obtained by integrating Eq. (16), as described by Eq. (19). The up component of velocity is usually damped by other height sensors and its error mechanism is changed. Correspondingly, only horizontal velocity errors are taken into account as well.

$$\begin{cases} \Delta V_E = \int_0^{\pi/\omega} \Delta f_E \mathrm{d}t \\ \quad = -\alpha_{ax} g \int_0^{\pi/\omega} \sin\omega t \mathrm{d}t + \beta_{ax} g \int_0^{\pi/\omega} \cos\omega t \mathrm{d}t \\ \quad = -\frac{2\alpha_{ax} g}{\omega} \\ \Delta V_N = \int_0^{\pi/\omega} \Delta f_N \mathrm{d}t \\ \quad = -\frac{\beta_{ay} g}{2} \int_0^{\pi/\omega} (1+\cos 2\omega t)\mathrm{d}t - \frac{\delta_{azX} g}{2} \int_0^{\pi/\omega} (1-\cos 2\omega t)\mathrm{d}t \\ \quad = -\frac{\beta_{ay} g \pi}{2\omega} - \frac{\delta_{azX} g \pi}{2\omega} \end{cases} . \quad (19)$$

3.2 *Navigation-Based Calibration Solution*

The error parameters listed above, except for α_{ax} and α_{ay}, have been corrected by a conventional method ahead of time; hence, the values of them become small in this calibration. For instance, the FOG scale factor errors can be reduced from several thousand parts per million (ppm) to dozens of ppm, and misalignment angles can be reduced from hundreds or thousands of arc seconds to several arc seconds. Based on this, Table 1 exhibits the pragmatic numerical relationship between error parameters and navigation errors in accordance with Eqs. (17) and (19), supposing $\omega = 6$ deg/s, $\omega_N = 11.49$ deg/h, $\omega_U = 9.64$ deg/h, and $g = 9.8$ m/s.

What deserve special attention are the impacts of ΔK_{gx} on $\Delta\phi_E$, δ_{gzY} on $\Delta\phi_N$, and α_{ax} on ΔV_E, since their values are a few orders of magnitude larger than others'. In line with Eq. (18), supposing the next time IMU rotating along with the Z_s axis is 2 min and the east angle error is 32.4″, the north velocity error that follows reaches up to 0.19 m/s, which is definitely apparent and unacceptable in high-precision INS. It is similar to the north angle error and the east velocity error. Furthermore, the noteworthy impacts are so decoupled that ΔK_{gx}, δ_{gzY}, and α_{ax} can be worked out

Table 1 Numerical relationship between error parameters and navigation errors.

Error parameter	Set value of error parameter	Navigation errors			
		$\Delta\phi_E$ (“)	$\Delta\phi_N$ (“)	ΔV_E (m/s)	ΔV_N (m/s)
ΔK_{gx}	50 ppm	**32.4**	0	0	0
β_{gx}	5”	−0.0053	0	0	0
β_{gy}	5”	0	−0.0035	0	0
δ_{gzX}	5”	0	−0.0035	0	0
δ_{gzY}	5”	0	**10**	0	0
β_{ay}	5”	0	0	0	−0.0036
α_{ax}	200”	0	0	**−0.18**	0
δ_{azX}	5”	0	0	0	−0.0036

Note: The largest values are indicated in bold.

effortlessly, which is helpful for the realization of calibration based on navigation.

Calculating the east velocity error ΔV_E in the course of IMU rotating along with X_s axis can directly help obtain the value of x accelerometer's installation error α_{ax} by Eq. (20), which is an expression of another form for Eq. (19).

$$\alpha_{ax} = -\frac{\Delta V_E \omega}{2g}. \tag{20}$$

While the value of α_{ax} is acquired in this way, α_{ay}, the other parameters that cannot be calibrated by conventional method can be calculated by Eq. (21).

$$\alpha_{ay} = (\alpha_{ay} - \alpha_{ax}) + \alpha_{ax}, \tag{21}$$

where $(\alpha_{ay} - \alpha_{ax})$ is obtained by a conventional method in advance.

Calculating the east velocity error ΔV_E in the followed course of IMU rotating along with Z_s axis can help obtain the north angle error $\Delta\phi_N$ by Eq. (18) first, and then z gyro's installation error δ_{gzY} would be obtained by Eq. (22), which is a simplification and variant of Eq. (17). Calculating the north velocity error ΔV_N in the same course can give an east angle error $\Delta\phi_E$ by Eq. (18), and x gyro's scale factor error ΔK_{gx} would be obtained by Eq. (22) subsequently.

$$\begin{cases} \Delta K_{gx} = \frac{1}{\pi}\Delta\phi_E \\ \delta_{gzY} = \frac{1}{2}\Delta\phi_N \end{cases}. \tag{22}$$

As velocity is also affected by the precision of alignment, this calibration is implemented by averaging the testing values of repeated measurements to reduce the impact of alignment error. Although not all of the error parameters can be calibrated using this approach, the key parameters that strongly damage a system's precision can be calibrated to a more advanced level.

4 Experimental Results and Discussion

4.1 *Experimental Method*

The dual-axis rotary FOG INS, which has been calibrated and compensated by conventional method, is placed on a stationary marble platform with the system's b-frame coincident with n-frame approximately (Fig. 3). The INS's inner axis is named Z_s axis, while the outer axis is named X_s axis. The system used in this experiment consists of three FOGs with an accuracy of 0.05 deg/h and three quartz accelerometers with an accuracy of 60 μg. It is fed by a dc-regulated power supply, and data are sampled by a laptop at a frequency of 20 Hz. According to the principle analyzed in Sec. 3, the INS works as follows.

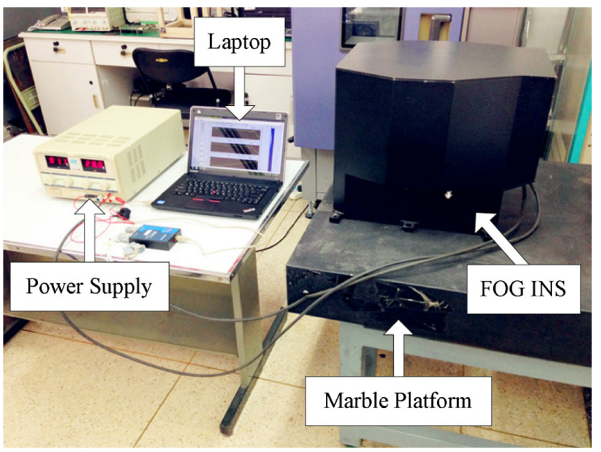

Fig. 3 The experimental setup.

After alignment, the navigation calculation starts, and the IMU rotates along with the Z_s axis first. Two minutes later, rotation along with the Z_s axis suspends and rotation along with the X_s axis executes for 30 s at a speed of 6 deg/s, which means the IMU rotates 180 deg along with the X_s axis. Then rotation along the Z_s axis continues, followed by rotation along the X_s axis in the inverse direction.

In the whole process, INS velocity is recorded for calibration. As it is carried out on a stationary base, velocity should be zero theoretically. So INS velocity just represents the velocity error and is treated as the measurement in calibration. This calibration must be completed in the first several minutes of navigation, because the accuracy of velocity decreases over operating time in INS. At the beginning, the measurement accuracy of velocity is usually better than 0.001 m/s. Take x gyro's scale factor error for example; according to Eqs. (18) and (22), the corresponding calibration error is ~0.3 ppm, which can be ignored.

4.2 *Calibration of x Accelerometer's Installation Error*

From the velocity output in the stationary base, we can get its velocity error directly. Figure 4 shows one calibration result for α_{ax} based on the east velocity error during IMU rotating along with X_s axis. During this process, which starts at the end of the second minute and ends a half minute later in Fig. 4(a), an east velocity error with the value of −0.113 m/s arises, meaning there is a misalignment angle of x accelerometer with a value of 124.2″ based on

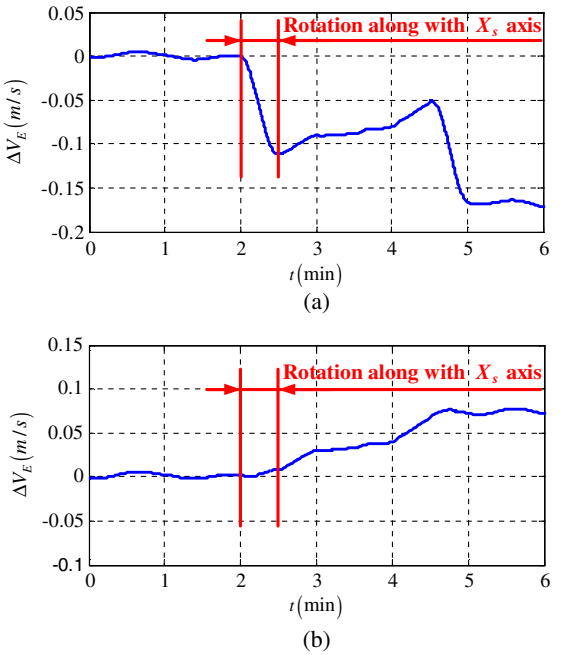

Fig. 4 Compare results of the east velocity error due to α_{ax}: (a) before calibration and (b) after calibration and compensation.

Table 2 Calibration results of α_{ax}.

Test number	ΔV_E (m/s) Rotation along with the X_s axis	α_{ax} (“)
1	−0.113	124.2
2	−0.110	121.5
3	−0.111	122.6
4	−0.107	117.9
5	−0.109	120.5
6	−0.109	119.7
Mean	**−0.110**	**121.1**
Root mean square	**0.002**	**2**

Table 3 Calibration results of δ_{gzY}.

Test number	ΔV_E (m/s) Rotation along with the Z_s axis	$\Delta\phi_N$ (“) Rotation along with the X_s axis	δ_{gzY} (“)
1	0.065	−11.4	−5.7
2	0.044	−7.6	−3.8
3	0.055	−9.7	−4.8
4	0.064	−11.2	−5.6
5	0.059	−10.3	−5.2
6	0.055	−9.6	−4.8
Mean	**0.057**	**−10.0**	**−5.0**
Root mean square	**0.008**	**1**	**0.7**

Eq. (20). Table 2 is a summary of calibration experimental results for α_{ax}. The mean of six results implies that the value of α_{ax} is $\sim 121.1''$, while the root mean square suggests the achievable calibration accuracy for α_{ax} is $\sim 2''$. After compensating α_{ax} using the mean value in Table 2, the obvious fluctuation of east velocity disappears as shown in Fig. 4(b).

4.3 *Calibration of **z** Gyro's Installation Error*

With the calibration and compensation of x accelerometer's installation error α_{ax}, the variation of east velocity is not as drastic as before, leaving z gyro's installation error δ_{gzY} as the dominant error source. In Fig. 5(a), during the rotation along with Z_s axis from 2.5 to 4.5 min, the east velocity error augments nearly 0.065 m/s, and a misalignment angle of z gyro with the value of $-5.7''$ can be figured out based on Eqs. (18) and (22). Six experimental calibration results are listed in Table 3, indicating that the residual value of δ_{gzY} after calibration and compensation by a conventional approach is some $-5''$, and its achievable accuracy is as good as $0.7''$. As shown in Fig. 5(b), correcting δ_{gzY} with $-5''$, the east velocity error stays near zero throughout the succedent rotation along with the Z_s axis.

4.4 *Calibration of **x** Gyro's Scale Factor Error*

Different from the two calibrations above, the calibration of the x gyro's scale factor error is based on the north velocity error. On account of the angle error engendered during rotation along with X_s axis due to ΔK_{gx}, a balloon of ~ 0.242 m/s happens to ΔV_N when IMU rotates along with the Z_s axis subsequently, as shown in Fig. 6(a). Utilizing Eqs. (18) and (22), the corresponding scale factor error with the value of 65.5 ppm can be worked out. Taking

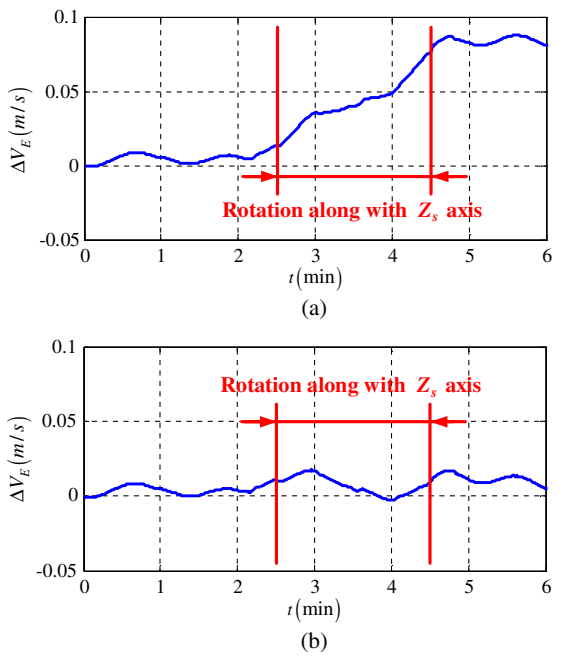

Fig. 5 Compare results of the east velocity error due to δ_{gzY}: (a) before calibration and (b) after calibration and compensation.

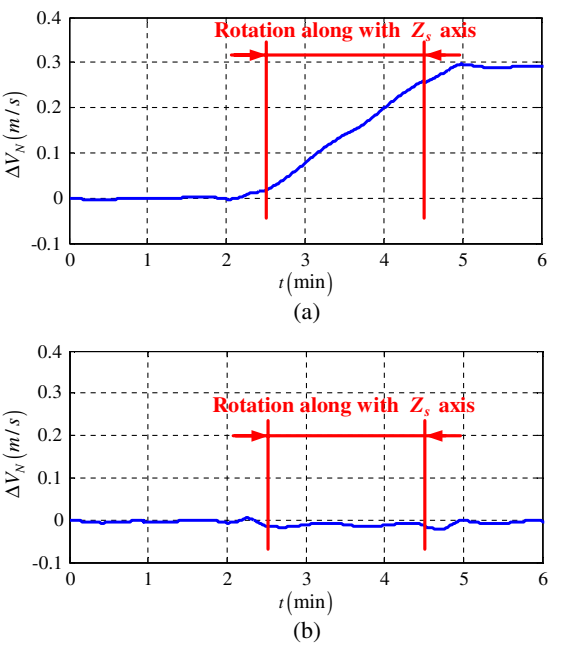

Fig. 6 Compare results of the north velocity error due to ΔK_{gx}: (a) before calibration and (b) after calibration and compensation.

Table 4 Calibration results of ΔK_{gx}.

Test number	ΔV_N (m/s) Rotation along with the Z_s axis	$\Delta\phi_E$ (") Rotation along with the X_s axis	ΔK_{gx} (ppm)
1	0.242	42.5	65.5
2	0.248	43.5	67.1
3	0.229	40.1	61.9
4	0.292	51.1	78.9
5	0.239	41.9	64.7
6	0.254	44.4	68.6
Mean	**0.251**	**43.9**	**67.8**
Root mean square	**0.02**	**4**	**6**

the same way, another five experimental results are received and recorded in Table 4. Using the mean value of 67.8 ppm for six results with an accuracy of 6 ppm to modify the x gyro's scale factor, the north velocity error is improved substantially.

4.5 *Discussion*

The experiments above are finished by the system's own operation, instead of mounting it on a high-accuracy turn table. In addition, the abscissas of Figs. 4(a), 5(a), and 6(a) indicate that this calibration method costs no more than 6 min, and, in contrast, conventional methods usually take as long as several quarters to calibrate these parameters. Both of the two points are in favor of this calibration's convenience. Although the impact of operating conditions on sensors is finite, the value of δ_{gzY} in Table 3 is only $\sim 5''$, and the value of ΔK_{gx} in Table 4 is only $\sim$67.8 ppm, they are not small enough and cause large navigation errors. Rapid accumulation of velocity errors disappear after calibration and compensation by the proposed technique, which suggests that this method is more accurate than conventional calibration in this system. The comparison of this calibration method with a conventional method is refined in Table 5.

Table 5 Comparison of calibration techniques.

	Multiposition and rotation calibration	Self-calibration method based on navigation
Dependence on external device	Yes	No
Execution time	Before navigation	In navigation
Parameters that can be calibrated	Almost all parameters	Key parameters
Time that calibration consumed	Several quarters	Several minutes
Accuracy that meets system requirement	Limited	High

5 Conclusion

A calibration approach based on the velocity error of stationary base navigation is presented for dual-axis rotary FOG INS in this paper. There are two uppermost advantages for this method. First, it is simple and practicable because it takes only several minutes and is implemented by its own rotating mechanism requiring no external device. Second, it is executed during the navigation process, namely, the status of IMU and the surroundings during calibration are the same as those during navigation, and the calibration results are more accurate compared with those obtained by a conventional method. One possible disadvantage is that not all error parameters can be calibrated. However, error parameters calibrated by this method, including x accelerometer's installation error, z gyro's installation error, and x gyro's scale factor error, are the fatal error sources in this type of inertial system. The accuracy of other parameters calibrated by conventional methods is also acceptable for this system. The experimental results show that high accuracies of $2''$ and $0.7''$ can be achieved for x accelerometer and z gyro's installation errors, respectively, while high accuracy of 6 ppm can be achieved for x gyro's scale factor error.

Acknowledgments

This study was supported by the Aeronautical Science Foundation of China (20110851007) and the Fund of BUAA for Graduate Innovation and Practice (YCSJ-01-2013-03).

References

1. S. Sabat et al., "Characterization of fiber optics gyro and noise compensation using discrete wavelet transform," in *Proc. 2nd Int. Conf. on Emerging Trends in Engineering and Technology*, pp. 909–913, IEEE, Nagpur (2009).
2. J. Nayak, "Fiber-optic gyroscopes: from design to production," *Appl. Opt.* **50**(25), E152–E161 (2011).
3. W. Sun et al., "MEMS-based rotary strapdown inertial navigation system," *Measurement* **46**(8), 2585–2596 (2013).
4. S. Ishibashi et al., "Accuracy improvement of an inertial navigation system brought about by the rotational motion," in *OCEANS 2007-Europe*, pp. 1–5, IEEE, Aberdeen, England (2007).
5. Y. F. Xu et al., "Error modeling and compensation for rotation-modulation strapdown inertial navigation system," *Adv. Sci. Lett.* **5**(2), 981–985 (2012).
6. W. Sun and Y. Gao, "Fiber-based rotary strapdown inertial navigation system," *Opt. Eng.* **52**(7), 076106 (2013).
7. K. M. Hays et al., "A submarine navigator for the 21th century," in *Position Location Navigation Symp.*, pp. 179–188, IEEE, California (2002).
8. B. L. Yuan, D. Liao, and S. L. Han, "Error compensation of an optical gyro INS by multi-axis rotation," *Meas. Sci. Technol.* **23**(2), 025102 (2012).
9. J. H. Cheng et al., "Research of strapdown inertial navigation system monitor technique based on dual-axis consequential rotation," in *IEEE Int. Conf. on Information and Automation*, pp. 203–208, IEEE, Shenzhen (2011).
10. R. Peesapati et al., "Efficient hybrid Kalman filter for denoising fiber optic gyroscope signal," *Optik* **124**(20), 4549–4556 (2013).
11. J. K. Bekkeng, "Calibration of a novel MEMS inertial reference unit," *IEEE Trans. Instrum. Meas.* **58**(6), 1967–1974 (2009).
12. T. Nieminen et al., "An enhanced multi-position calibration method for consumer-grade inertial measurement units applied and tested," *Meas. Sci. Technol.* **21**(10), 105204 (2010).
13. A. M. Kurbatov and R. A. Kurbatov, "Temperature characteristics of fiber-optic gyroscope sensing coils," *J. Commun. Technol. Electron.* **58**(7), 745–752 (2013).
14. Z. H. Li et al., "A novel method for determining and improving the quality of a quadrupolar fiber gyro coil under temperature variations," *Opt. Express* **21**(2), 2521–2530 (2013).
15. D. W. Zhang et al., "Magnetic drift in single depolarizer interferometric fiber-optic gyroscopes induced by orthogonal magnetic field," *Opt. Eng.* **52**(5), 054403 (2013).

16. Y. G. Zhang and Z. X. Gao, "Fiber optic gyroscope vibration error due to fiber tail length asymmetry based on elastic-optic effect," *Opt. Eng.* **51**(12), 124403 (2012).

Lei Wang is a PhD candidate in precision instrument and machinery at Beihang University. He received his BEng from the School of Instrumentation Science and Opto-electronics Engineering, Beihang University in 2009. His research interests are in inertial navigation, motor control, and so forth.

Wei Wang received her PhD from Northwestern Polytechnical University in 2005. From 2005 to 2007, she was a postdoctoral fellow at the School of Instrumentation Science and Opto-electronics Engineering, Beihang University, where she is currently an associate professor. Her research fields include inertial navigation, satellite navigation, and integrated navigation.

Qian Zhang is a PhD candidate in precision instrument and machinery at Beihang University. He received his BEng from the School of Instrumentation Science and Opto-electronics Engineering, Beihang University in 2012. His research interests include inertial navigation.

Pengyu Gao is a PhD candidate in precision instrument and machinery at Beihang University. He received his BEng from the School of Advanced Engineering, Beihang University in 2012. His research interests are in inertial navigation, big data, and so forth.